Electron Injection Dynamics of Ru Polypyridyl Complexes on SnO_2 Nanocrystalline Thin Films

Xin Ai, Neil A. Anderson,§ Jianchang Guo, and Tianquan Lian*

Department of Chemistry, Emory University, Atlanta, Georgia 30322

Received: September 1, 2004; In Final Form: December 10, 2004

Ultrafast infrared spectroscopy was utilized to investigate the electron-transfer dynamics from $Ru(dcbpy)_2(X)_2$ complexes (dcbpy = 4,4′-dicarboxy-2,2′-bipyridine; $X_2 = SCN^-$, $2CN^-$, and dcbpy; referenced as RuN3, Ru505, and Ru470, respectively) to nanocrystalline SnO_2 films. For both films exposed to air (dry) and submerged in a pH 2 buffer solution, all traces show biphasic dynamics with a small ultrafast component (less than 10%) and nonexponential slow component, indicating that most injection occurs from thermalized excited state of the dye. In the dry film, the injection rate becomes slower, comparing RuN3, Ru505, and Ru470, correlating with decreasing excited-state oxidation potentials in these dyes. However, the variation of injection rate with dye potential is less noticeable at pH 2. The possible reason for the different injection dynamics in these dyes and under different environments are discussed. These injection dynamics are also compared with those on TiO_2 and ZnO.

Introduction

Interfacial electron transfer (ET) dynamics of molecular adsorbate/semiconductor nanoparticle systems has been investigated intensely in recent years. The interest has stemmed from the desire to obtain a fundamental understanding of the process as well as the practical need to improve dye-sensitized solar cell (DSSC) performance.[1−4] In a DSSC device, charge separation and recombination dynamics at the adsorbate/semiconductor interface play a crucial role in determining the overall cell efficiency.[5,6] Solar cells based on $Ru(dcbpy)_2(NCS)_2$ (abbreviated as RuN3, dcbpy = 4,4′-dicarboxy-2,2′-bipyridine)-sensitized TiO_2 nanocrystalline porous films have demonstrated a high light-to-electric energy conversion efficiency of about 10%,[5,7] and near unity of incident-photon-to-current conversion efficiency (IPCE) value at the peak wavelength.[4,8,9] For this reason, ET in the RuN3/TiO_2 system has been extensively studied[10−23] and is known to occur on the ultrafast time scale, consisting of a fast component (<100 fs) and one or more slower components on the picosecond and longer time scale. The fast component corresponds to injection from unthermalized excited state, which competes with intramolecular vibrational energy redistribution and relaxation and intersystem crossing within the excited-state manifold. The picosecond scale components correspond to injection from relaxed ^{3}MLCT states near the conduction band edge.[10] The charge recombination is found to occur on a much slower time scale, from microsecond to millisecond.[18,22,24] The high conversion efficiency and IPCE can be partly attributed to efficient ultrafast charge separation and slow recombination.

Recently, SnO_2, another stable wide band gap semiconductor, has also been explored as a substitute for TiO_2 in dye-sensitized solar cells.[25−31] The conduction band of SnO_2 lies about 0.5 V less negative than that of TiO_2,[4] rendering the electron transfer from dye to SnO_2 energetically more favorable. A wide variety of organic and organometallic molecules, including chlorophyll,[29,32,33] metalloporphyrins[34,35] and porphyrin-C60 dyad,[25] perylene,[31] mercurochrome,[36] cyanine dyes,[37−39] and Ru polypyridyl complexes,[27,28,30,40−42] have been utilized to sensitize nanocrystalline SnO_2 electrodes. However, unlike TiO_2, the injection processes from dye to SnO_2 is less intensely investigated and there is still a lack of knowledge about injection dynamics on SnO_2. Iwai et al. reported that interfacial charge separation takes place from both singlet and triplet MLCT of $Ru(bpy)_2(dcbpy)$ adsorbed on SnO_2.[43] Benko[44] and Bauer[45] observed nonexponential dynamics but with significantly varied rates. Early studies in our group[11] have reported that injection dynamics from RuN3 to SnO_2 is dominated by the picosecond components.[11−13] To further understand the injection dynamics on SnO_2 nanocrystalline thin films, in this work we investigated its dependences on excitation power density, dye energetics, and sample environment using ultrafast infrared spectroscopy. The transfer rate as a function of adsorbate excited-state oxidation potential was tested by using $Ru(dcbpy)_2(X)_2$ compounds (dcbpy = 4,4′-dicarboxy-2,2′-bipyridine, $X_2 = 2SCN^-$, $2CN^-$ and dcbpy, abbreviated as RuN3, Ru505, and Ru470, respectively) and comparing different film surface environments (dry and pH 2).

Experimental Section

Preparation of SnO_2 Colloid and Films. Colloidal SnO_2 was synthesized according to a published procedure.[46,47] Briefly, 0.085 mol of $SnCl_4$ was dissolved in 20 mL of HCl (37 wt %). The resulting solution was allowed to cool to room temperature and added dropwise into 500 mL of water under vigorous stirring at 0 °C. Aqueous ammonia (25%) was added to the solution until a pH value of 3.5 was reached, which results in the precipitation of SnO_2 nanoparticles. The white precipitate was washed at least three times with distilled water and added into 300 mL of water, onto which aqueous ammonia was added to adjust the pH value to 9.5−10. The solution was stirred overnight and dialyzed against 10 L of aqueous ammonia at pH 10. The resulting transparent SnO_2 colloid was refluxed for 4 h. A 100 mL aliquot of this colloid was poured into an

* To whom correspondence should be addressed. E-mail: tlian@emory.edu.
§ Present address: National Institute of Standards and Technology, Gaithersburg, MD 20899-8443.

10.1021/jp046037d CCC: $30.25
Published on Web 03/29/2005

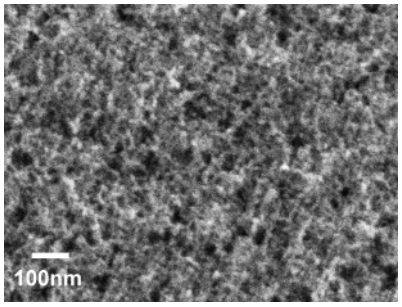

Figure 1. SEM image of a SnO_2 nanocrystalline thin film.

autoclave and heated at 150 °C for 1 h and then at 270 °C for 16 h. The solution was then concentrated to 30 mL, and 15 drops of TritonX-100 were added. After 1 day of stirring, the solution was cast onto sapphire substrates and dried in air. The thin films were baked at 400 °C for 1 h and then allowed to slowly return to room temperature. The resulting films were about 2−5 μm in thickness and showed good transparency. The SEM image of the film (Figure 1) indicates a nanoporous network composed of ∼10 nm diameter particles.

Sensitization of Semiconductor Films. High-purity RuN3, Ru505, and Ru470 were purchased from Solaronix (Lausanne, Switzerland). SnO_2 films were sensitized by soaking in dye solutions, followed by rinsing off unbound molecules using the solvent. The concentration of RuN3 ethanolic solution was about 1 mg/mL, and for Ru505 and Ru470, a saturated aqueous solution was used. Typically, films were soaked 5−10 min in RuN3 solution to obtain an optical density of 0.2−0.4 at 400 nm, corresponding to 6−11% dye coverage compared to the highest uptake of RuN3 by the SnO_2 film. Because Ru505 and Ru470 solutions are much less concentrated, films were sensitized overnight to obtain the equivalent absorption. For experiments performed at pH 2, the sensitized films were soaked in pH 2 buffer for at least 4 h and were kept in contact with a small volume of the buffer during the transient absorption measurement.

Ultrafast Infrared Transient Absorption Measurements. Ultrafast experiments were carried out in a pump−probe transient absorption scheme, and the details of the setup have been reported previously.[48,49] Briefly, the tunable infrared spectrometer used for the study utilizes a 1 kHz regeneratively amplified Ti:sapphire laser system (800 nm, 100 fs, 900 μJ/pulse). Difference frequency generation from the signal and idler of an IR optical parametric amplifier (OPA) produced the tunable mid-IR probe pulses with a ∼250 cm^{-1} bandwidth. Pump pulses at 400 nm were provided by second harmonic generation (SHG).

The pump beam had a spot size of 500 μm at the sample, whereas the mid-IR probe beam was focused to 300 μm at the sample. The probe was dispersed in a spectrometer and detected using a 32-element MCT array detector. The spectral resolution was 15 nm (∼6 cm^{-1} at 2100 cm^{-1}). Zero time delay was defined and the instrument response was characterized utilizing a CdS film, which gives an instantaneous mid-IR absorption response to the pump beam. Typically, the instrument response at the sample was well characterized by a 200 fs fwhm Gaussian function. During data collection, samples were constantly translated to avoid accumulation of permanent photoproducts.

Results

UV−Vis Absorption. Figure 2 shows the UV−vis absorption spectra of RuN3-sensitized and unsensitized SnO_2 films. For comparison, the absorption spectrum of RuN3 in ethanol solution is presented as well. Two bands attributed to metal-to-ligand charge-transfer (MLCT) transition are observed at 537 and 398 nm for RuN3 in ethanol. When absorbed onto SnO_2 film, the bands blue shift to 517 and 385 nm, respectively. A similar blue-shifted absorption has been observed for N719 (partially deprotonated version of RuN3) on SnO_2 film compared to its ethanol solution.[45] This blue shift likely originates from deprotonation of the −COOH groups in RuN3 after absorbed onto SnO_2 film and/or solvatochromic shift from ethanol to air.[50]

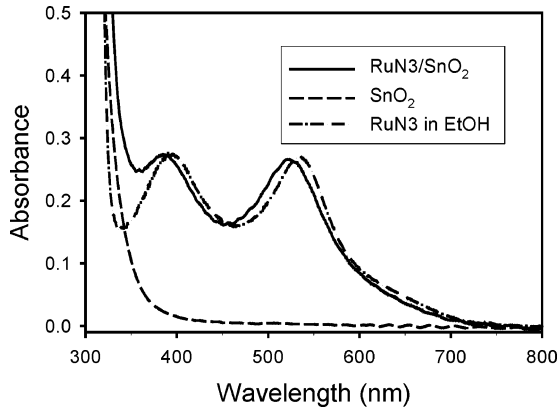

Figure 2. UV−vis absorption spectra of RuN3-sensitized SnO_2 film (solid line), unsensitized SnO_2 film (dashed line) and RuN3 in ethanol solution (dash−dotted line).

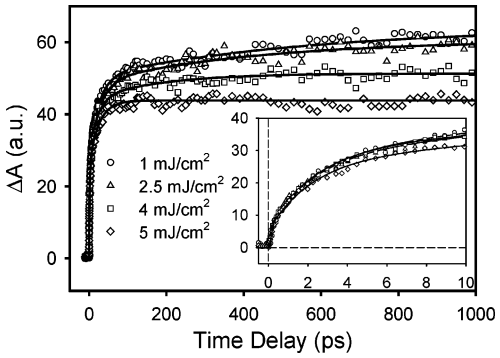

Figure 3. Kinetic traces of RuN3/SnO_2 (pH 2) probed at 2000 cm^{-1} using four different 400 nm excitation densities (as indicated on the figure) and normalized by corresponding pump power. The inset expands the early delay time dynamics.

Pump-Power Dependent Measurement. The effect of excitation density on injection dynamics was investigated by testing RuN3-sensitized SnO_2 film at pH 2 using four different 400 nm excitation densities (1, 2.5, 4, 5 mJ/cm^2 per pulse). Kinetic traces were probed at 2000 cm^{-1}, where contributions from the dye vibrational modes is negligible, thus reflecting the dynamics of electrons injected to the semiconductor.[11,46,47] The electron signals normalized by corresponding pump powers are plotted in Figure 3 to compare the relative yield and dynamics. From 5 to 2.5 mJ/cm^2, the apparent injection rate decreases, but the relative yield observed at 1 ns increases. In contrast, the dynamics for the lowest two pump intensities (1 and 2.5 mJ/cm^2) were virtually identical and the yield depended linearly on intensity. The inset in Figure 3 expands the early-time dynamics, demonstrating that all traces were nominally identical within 2 ps, with differences occurring on longer time scales. The origin of this pump-power dependence will be discussed later and the following measurements were all performed with 1 mJ/cm^2 400 nm pulses to avoid nonlinear response at higher power.

SCHEME 1: Two-State Injection Model[a]

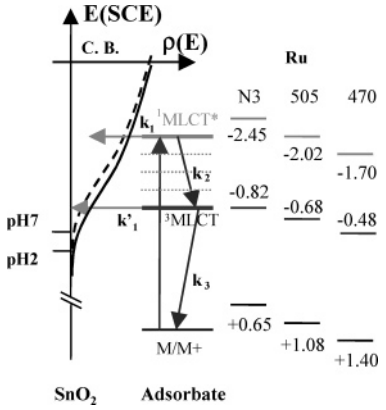

[a] The oxidation potentials for the ground and excited state (unthermalized and thermalized) of Ru dyes are shown as well. The oxidation potentials are adopted from ref 10 and references within. Values of the ^{1}MLCT state are calculated on the basis of 400 nm excitation.

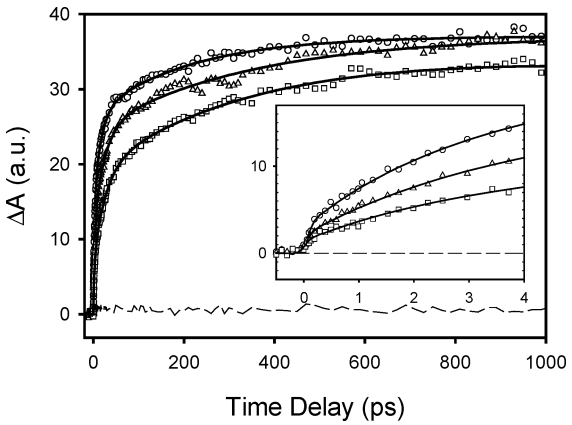

Figure 4. Absorption-normalized injected electron traces (symbols) and fits (solid lines) probed at 2000 cm^{-1} for RuN3 (circles), Ru505 (triangles) and Ru470 (squares) on SnO_2 dry films. The SnO_2 blank film signal is shown as a dashed line in the main panel and has already been subtracted to give the displayed traces. The fitting functions are discussed in the text and parameters are listed in Table 1. The inset expands the early delay time dynamics.

Injection Dynamics from Ru Dyes to SnO_2. Three Ru complexes, RuN3, Ru505 and Ru470 were used here to investigate ET to nanocrystalline SnO_2 film. Use of these specific molecules allows exploration of the effects of adsorbate energetics on ET, and the series has previously been studied on TiO_2[10,11,51] and Nb_2O_5.[52] Ru505 and Ru470 have the same dcbpy ligand as RuN3, only differing in the third pair of coordination ligands X ($2X = 2SCN^-$, CN^- and dcbpy for RuN3, Ru505 and Ru470, respectively), which accounts for significant changes in their energetics. From RuN3 to Ru505 to Ru470, the ground-state and excited-state oxidation potentials become less negative,[10,51] as shown in Scheme 1.

Figure 4 demonstrates the electron injection kinetics of Ru dyes on SnO_2 dry films probing at 2000 cm^{-1} after 400 nm excitation. The unsensitized SnO_2 blank film signal is shown in Figure 4 as a dashed line and has already been subtracted to give the displayed traces. The inset expands the early time dynamics. The noise level introduced by film inhomogeneity is about 10−15%. These traces have been scaled to correspond to the same number of photons absorbed by the dyes, allowing quantitative comparison of relative signal size and thus the injection yield. The 1 ns injection yields are similar for RuN3 and Ru505, whereas for Ru470 it is about 85% of that for RuN3. All traces show biphasic dynamics and were fit using a multiexponential rise convoluted with the instrument response function. The time scales and relative amplitudes of the fit are listed in Table 1 as τ (ps) and A (%). The fitting shows a small (<10% in amplitude) ultrafast (<100 fs) component for all the samples. The slow rise was fit by a three-exponential function and the average rate of the slow components was calculated by eq 1. From RuN3 to Ru505 to Ru470, the average rate of slow components decreases.

TABLE 1: Fitting Parameters for Ru Dyes/SnO_2 Kinetics[a]

	fast A% (<100 fs)	A_1, τ_1 (%, ps)	A_2, τ_2 (%, ps)	A_3, τ_3 (%, ps)	τ_{slow}, ps
RuN3/SnO_2 dry	8.9	29.3, 2.5	33.7, 15.8	28.1, 212	72
Ru505/SnO_2 dry	6.2	24.6, 3.1	35.4, 23.7	33.8, 339	132
Ru470/SnO_2 dry	3.8	14.8, 2.6	32.6, 26.5	48.8, 371	198
RuN3/SnO_2 pH2	6.8	28.5, 2.0	31.3, 19.5	33.4, 377	142
Ru505/SnO_2 pH2	4.7	20.2, 2.6	32.3, 20.0	42.8, 418	195
Ru470/SnO_2 pH2	5.1	20.8, 2.6	35.4, 24.0	38.7, 400	173

[a] Amplitudes and time scales for the multiexponential fits shown in Figures 4 and 5. The slow rise amplitudes are represented by A_1, A_2 and A_3 and their corresponding time scales are τ_1, τ_2, and τ_3. The values for τ_{slow} are calculated as a weighted average of the slow component time constants according to eq 1.

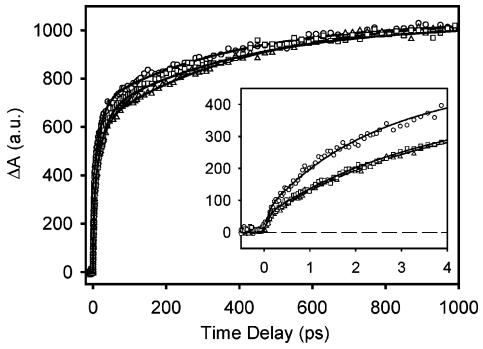

Figure 5. Comparison of normalized injected electron traces (symbols) and fits (solid lines) probing at 2000 cm^{-1} for RuN3 (circles), Ru505 (triangles) and Ru470 (squares) on SnO_2 at pH 2. The fitting functions are discussed in the text and parameters are listed in Table 1. The inset expands the early delay time dynamics.

$$\tau_{slow} = \frac{A_1\tau_1 + A_2\tau_2 + A_3\tau_3}{A_1 + A_2 + A_3} \quad (1)$$

The ET rate was also measured at pH 2, at which the conduction band edge position of SnO_2 is lowered compared to that of the dry film due to the pH dependence of band edge position.[53] This allows testing the effect of sensitizer energetics on injection dynamics (shown in Scheme 1). Interestingly, after scaling the kinetic traces at pH 2 to correspond to the same number of absorbed photons (data not shown here), the relative signal sizes for Ru505 and Ru470 are identical, whereas the signal size for RuN3 is about 25% lower even though the apparent dynamics of RuN3 are slightly faster than both Ru505 and Ru470, as shown from the size-normalized traces in Figure 5. The reason for the lower RuN3 yield at 1 ns is as yet unclear and may result from either RuN3 molecules that are unable to inject under these conditions or from injection components that are slow compared with the 1 ns window of the present experiment. For the purposes of comparison, we plot all traces of Ru dyes on SnO_2 at pH 2 by normalizing the signal size at 1 ns (Figure 5) and fit the traces using a multiexponential rise function. The fitting parameters are listed in Table 1 as well. These traces are also shown to be biphasic, dominated by slow components with small portion of ultrafast (<100 fs) component.

Compared to the dry film results, the rate difference among three dyes is less prominent. RuN3 still demonstrates the fastest dynamics; however, the dynamics for Ru505 and Ru470 are quite similar.

Discussion

Pump-Power Dependence. The pump-power dependent behavior of RuN3/SnO_2 is suspected to arise from quenching of excited molecules through triplet−triplet annihilation. A dye molecule in its singlet excited state (created by photoexcitation) quickly relaxes to a triplet state. If the excitation density is high enough, some molecules in their triplet excited states may interact with each other, returning one to the ground state and promoting the other to a singlet excited state. The new-formed singlet excited state will relax rapidly to the triplet state, resulting annihilation of triplet excited states as presented by eq 2.[54]

$$^3M^* + {}^3M^* \rightarrow {}^1M^* + {}^1M \rightarrow {}^3M^* + {}^1M \qquad (2)$$

Therefore, the slow injection component is diminished due to the depopulation of the relaxed excited state. This results in a relatively lower yield and faster observed dynamics at higher excitation density due to a smaller slow component amplitude. Excited-state quenching on the similar time scale has been observed by Shaw and Papanikolas in related Ru polypyridyl complexes.[54] Under our experimental condition, quenching processes can be eliminated by using excitation power of less than 2.5 mJ/cm^2, as shown in Figure 3.

Correlation of Electron Signal to Injection Dynamics. The signal measured here corresponds to the absorption of injected electron in semiconductor, which has been used as a probe of electron transfer from dye to TiO_2, ZnO, and SnO_2 semiconductor thin films.[11,14,46,55,56] The electron absorption signal depends on both the population dynamics and absorption cross-section change in the semiconductor.[10] When the latter is negligible, the measured electron signal can be used directly to monitor the injection dynamics. In cases where slower injection from the dye relaxed excited state dominates, electron cross section decay has generally been observed to be minimal.[46,48,55,56] This is likely due to injection occurring near the semiconductor band edge, reducing the excess kinetic energy of the injected electrons. Previously, we have reported that on ReC1A [Re(CO)3Cl(L′), L′ = 4,4′-diacetate-2,2′-bipyridine]-adsorbed SnO_2 film the injected electron dynamics correlated very well with oxidized molecule signal, indicating no detectable cross-section decay, and electron transfer was measured to take place on 40 ps time scale with negligible fast component.[46] Energetically ReC1A and RuN3 are similar,[10] and the electron traces of Ru dye-sensitized SnO_2 films measured here only shows a small amplitude of fast component and are dominated mostly by slow dynamics. Therefore, we assume that the cross-section decay is negligible and that the electron signal provides a direct measurement of injection dynamics in the systems studied here.

Biphasic Injection Dynamics. As in RuN3 sensitized TiO_2, ZnO and Nb_2O_5,[10,52,56] electron injection from Ru dyes to SnO_2 films also shows biphasic kinetics. Again, the fast (<100 fs) component is attributed to injection from the unthermalized ^{1}MLCT excited state, which is competitive with intramolecular vibrational energy redistribution and relaxation as well as intersystem crossing (ISC). The slow components correspond to injection from relaxed ^{3}MLCT states near the conduction band edge. Similar biphasic dynamics and attribution have been reported for injection to SnO_2 from RuN3[44] and Ru(bpy)2(dcbpy)[43] complexes by other groups. We have proposed a two-state injection model previously to account for the biphasic injection kinetics in RuN3 on TiO_2, ZnO and Nb_2O_5.[10,52,56] According to this model (shown in Scheme 1), electron injection can occur from ^{1}MLCT and ^{3}MLCT excited states with a rate constant of k_1 and k_1', respectively, and it competes with the relaxation (with a rate constant of k_2) from ^{1}MLCT to ^{3}MLCT. If $k_1 \gg k_1'$, the electron population in semiconductor is given by

$$N_e(t) = N_0\left[\frac{k_1}{k_1+k_2}(1 - e^{-(k_1+k_2)t}) + \frac{k_2}{k_1+k_2}(1 - e^{-k_1't})\right] \qquad (3)$$

where N_0 is the total number of excited molecules that are able to undergo electron transfer. The first term corresponds to injection from the unthermalized excited state, and the second term to injection from the relaxed excited state. Branching between hot excited-state injection and dye relaxation is therefore controlled by the ratio of k_1/k_2. Though the rate of the fast component is much faster than our instrument resolution and cannot be resolved here, its amplitude reflects the rate of injection from unthermalized excited states due to the competition between injection and relaxation processes. In contrast to TiO_2, for which injection is dominated by the fast component,[10,13,14] the much smaller fast component measured here suggests that ^{1}MLCT excited-state injection rate to SnO_2 is much slower and that most transfer originates from the ^{3}MLCT excited state. This noticeable difference of injection dynamics observed on different semiconductor films will be discussed later.

Comparing Rate Constants of RuN3/SnO_2 from Different Studies. Here the electron injection dynamics on RuN3/SnO_2 is shown to be dominated by slow components with a small fast component, qualitatively consistent with our previous observation on RuN3/SnO_2 dry film.[11] The slightly different dynamics of slow injection between the two studies is ascribed to the effects from different testing conditions (such as pump power) and different batches of SnO_2 films. We have shown that the preparation condition of films affects the slow injection significantly, especially for injection close to the conduction band edge.[56] The band edge for dry SnO_2 film is unknown, but it is expected to be more negative than −0.3 V (vs SCE), the position at pH 7, due to its dependence on interfacial proton concentration.[53,57,58] As shown in Scheme 1, the relaxed excited-state redox potential of RuN3 is near the conduction band edge of SnO_2, where defect states may influence slow injection notably and differ from batch to batch.

As we mentioned above, Benko et al.[44] measured transient absorption at 850 nm and observed a similar biphasic injection from RuN3 to SnO_2 and TiO_2 with only slightly less fast component on SnO_2, which is quite different from what we observed here or previously. Several factors may contribute to this discrepancy. First, they tested samples in acetonitrile instead of exposing to air or in pH 2 solution as studied here. Different film environments may change the flatband potential V_{fb} of semiconductor[53] and reorganization energy,[59] which can also change the injection dynamics dramatically. A systematical investigation of solvent effect is underway, which hopefully will lead to an understanding of the contradictory results reported from different studies. Second, as shown in Figures 4 and 5, the injection kinetics appear to continue to grow beyond 1 ns, the longest time delay investigated. The final amplitude is extrapolated from fitting the data within the 1 ns window. The fast component amplitude calculated this way likely represents an upper limit and is severely overestimated if there are ≫1 ns injection components. It is likely that a similar (and perhaps more severe) problem exists in the estimate by Benko and co-

workers whose data extend to only 200 ps.[44] Third, there may be significant differences in the nanoporous films prepared in different groups, which can lead to a noticeable change of injection processes to states near the band edge, as was observed in ZnO,[56] TiO_2[10] and Nb_2O_5.[52] This sensitivity to sample and measurement conditions has also been observed by Kallioinen et al.[60]

Influence of Adsorbate Energetics on Injection Dynamics. For the electron injection in weak coupling limit, the transfer rate from an adsorbate to semiconductor may be expressed as the sum of ET rates to all possible accepting states in the semiconductor:[11,61−63]

$$k_{ET} = \frac{2\pi}{h}\int_{-\infty}^{\infty} dE\rho(E)|\overline{H}(E)|^2 \frac{1}{\sqrt{4\pi\lambda k_B T}} \times \exp\left[-\frac{(\lambda + \Delta G_0 + E)^2}{4\lambda k_B T}\right] \quad (4)$$

where $\Delta G_0 = E_{CB} - E_{ox}(s^*)$ is the energy difference between the conduction band edge and the oxidation potential of adsorbate excited state, $\rho(E)$ is the density of semiconductor states at energy E from the conduction band edge, $H(E)$ is the average electronic coupling between the adsorbate excited state and different k states in the semiconductor at the same energy E, and λ is the total reorganization energy.

Nevertheless, an inhomogeneous distribution of adsorbate and semiconductor properties, such as varying surface stoichiometry,[64] local energetics,[65] and binding geometry, likely exists, leading to a distribution of electronic coupling matrix elements[66] or density of states,[65] and introducing a nonexponential injection process. Experimentally, non-single-exponential dynamics has been commonly observed for interfacial ET from sensitizer to semiconductors,[11,16,20,23,46,52,56,65,67] including SnO_2.[44−46] In this work, the non-single-exponential dynamics from Ru complexes to SnO_2 films were fit by a three-exponential rise function, which does not necessarily imply that there are only three different injection rates. Instead, there may be a broad distribution of rates. Therefore we compare the amplitude weighted average rate, as defined in eq 1, of these kinetics.

For simplicity, we assume that in the region of interest, the density of states in semiconductor conduction band is described by a simple band characterized by a nearly-free electron model with effective mass m^*. According to eq 4, the interfacial ET rate depends on the density of accepting states in the semiconductor as well as electronic coupling and reorganization energy. Assuming that the effective electronic coupling is independent of the energy, the dependence on the semiconductor density of states leads to a variation of ET rate with the relative energetic of adsorbate excited state and conduction band edge, $E_{CB} - E_{ox}(s^*)$. To illustrate this dependence, we have computed ET rate as a function of $E_{CB} - E_{ox}(s^*)$ at different λ values using eq 4. We assume that the density of states near the band edge is described by

$$\rho_0(E)\,dE = \frac{(2m^*)^{3/2}}{2\pi^2\hbar^3}\sqrt{E}dE \quad (5)$$

where m^* is the effective mass of electrons in the conduction band ($m^* \sim 0.3$ of rest mass of electron for SnO_2).[68] We have neglected the contribution from surface states or defect states below the band edge. Inclusion of defect states, which is often modeled as an exponential tail extending below the band edge,[68,69] leads to only small changes above the band edge. As shown in Figure 6, the injection rate increases when the adsorbate excited state is further above the conduction band edge (more negative value of $E_{CB} - E_{ox}(s^*)$. The rate change is small high above the band edge but is nearly exponential close to the band edge, reflecting the energy dependence of conduction band density of states.

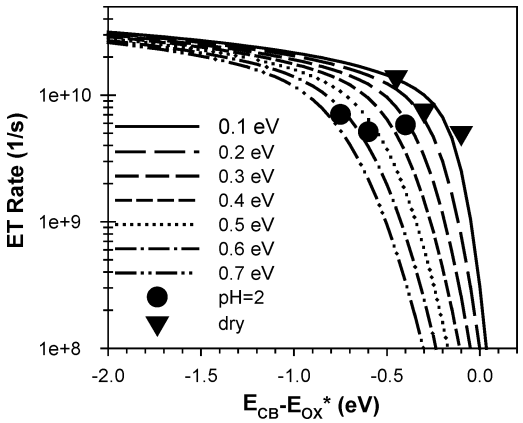

Figure 6. Calculated density of state (thin curve) of and ET rate (symbols) to SnO_2 as a function of $E_{CB} - E_{ox}(s^*)$ (energy difference between semiconductor conductor band edge and excited-state oxidation potential) under different reorganization energy according to eq 4.

The Ru complexes used in this work are attached to SnO_2 through the dcbpy ligand. If these complexes have similar electronic coupling between their dcbpy π^* orbital and the semiconductor, and similar reorganization energy, the rate difference can be attributed to their different oxidation potential. To test whether energetic consideration alone is sufficient to account for the different injection rate, we compare the measured rates with calculated rates. The measured rate is computed from the average injection times. The oxidation potentials (of the relaxed excited state) of three Ru dyes are listed Scheme 1. The conduction band edge for SnO_2 is about -0.06 V vs SCE at pH 2 and increases by -0.059 V per pH unit.[70,71] The position of the dry film (which is exposed to air) is not clear and is assumed to be the same as that at pH 7. The inner sphere reorganization energy of related Ru bipyridyl complexes have been shown to be negligible.[72] Treating the sample at pH 2 and dry conditions as SnO_2/water and SnO_2/vacuum interfaces, and using the dielectric continuum model[73] (with static and optical dielectric constants of 13 and 4 for SnO_2, 78 and 1.78 for water, and 1 and 1 for vacuum and spherical cavity radius of 6.8 Å for Ru complexes[74]), the solvent reorganization energy is estimated to be 0.46 and 0.13 V for pH 2 and dry films, respectively.

To compare the rate computed from eq 4 and the measured rate, the coupling strength is allowed to change until the calculated curve for $\lambda = 0.1$ eV agrees with the measured rate for dry film, as shown in Figure 6. It appears that the trend of injection rate from these dyes to SnO_2 dry film is reasonably well accounted for by considering their excited-state oxidation potential difference. However, for the samples at pH 2, the observed rates do not agree with the prediction of eq 4. It may indicate a noticeable variation of the outer sphere reorganization energy in these complexes and/or their electronic coupling strength with the semiconductor. It is also interesting to note that the observed rate change from dry film to pH 2 buffer reflects the competing effects of solvents, which affect both the conduction band edge position and reorganization energy. At pH 2 buffer, the effect of lowered conduction band edge (which would lead to an increase in injection rate if other parameters

remained constant) is offset by the increase in reorganization energy (which would lead to a decrease in rate).

Comparison of Injection Dynamics in SnO_2 with TiO_2 and ZnO. The injection dynamics from RuN3 to TiO_2, ZnO and SnO_2 are all biphasic, consisting of a <100 fs and picosecond scale components, which correspond to the injection from both unrelaxed ^{1}MLCT and relaxed ^{3}MLCT excited states of dye, respectively. As we discussed above, although the rate of the fast component cannot be resolved, the amplitude of the fast component reflects the injection rate from hot excited and can be compared

In contrast to TiO_2, a much smaller fast component for RuN3 on SnO_2 suggests a slow transfer rate from the RuN3 ^{1}MLCT excited state, which is estimated to be 1 order of magnitude slower than that to TiO_2 according to the two-state model. Because the conduction band edge position of SnO_2 is ~0.5 V lower than that of TiO_2,[4] the energetic difference is unable to account for the slower transfer rate on SnO_2. Instead, it is suspected to arise from the differences in the conduction band electronic structures.[11,52,75] The SnO_2 conduction band is composed primarily of empty s (and p) orbitals of Sn^{4+},[64] whereas that of TiO_2 is composed primarily of empty d orbitals of Ti^{4+}.[64,76] Typically, sp bands are broader and have density of states orders of magnitude lower than d bands.[64,68,77] From the effective mass of the conduction band electron in TiO_2 (5−10 m_e) and SnO_2 (0.3 m_e),[57,78] the density of conduction band states at the energy level of the Franck−Condon state prepared by 400 nm excitation (−2.4 V vs SCE) is estimated to be 2 orders of magnitude higher in TiO_2 than in SnO_2.[68] The relative injection rate from the unthermalized excited state appears to correlate with this trend of density of states. However, for the injection from the thermalized excited state of RuN3 to TiO_2 and SnO_2, the density of states difference may not be as big as for hot electron injection, because the injection state is still high above the SnO_2 band edge, but closer to the TiO_2 conduction band edge, where the density of states decreases dramatically. Therefore, it is possible to observe a similar rate of slow components to both materials.

Previously, we have measured injection dynamics from RuN3 to ZnO, another semiconductor with sp type conduction band, whose band edge is close to TiO_2, about 0.5 V higher than that in SnO_2.[4] Similarly, the injection to ZnO has a small fast component (<14%) and is dominated by a slow component,[56] which is several times slower than to SnO_2. The relaxed excited state of RuN3 is near the band edges of ZnO but high above that in SnO_2. A higher density of accepting states is expected in SnO_2, accounting for the relatively faster injection rate at the picosecond time scale than that in ZnO.

Summary

The injection dynamics from three Ru polypyridyl complexes with different energetics to nanocrystalline SnO_2 films were compared at both dry and pH 2 conditions. All traces show biphasic dynamics, with a small ultrafast component (less than 10%) and nonexponential slow component, indicating most injection occurs from the thermalized excited state. Comparing RuN3, Ru505, and Ru470 shows that the rates of both the fast and slow components slow in correlation with less negative excited-state oxidation potentials in these dyes. However, the injection rate difference at pH 2 is not as substantial as that on dry films. Comparing injection from RuN3 to different semiconductors, we find that the amplitude of the fast component on SnO_2 is similar to that on ZnO but much smaller than that on TiO_2, suggesting a significantly slower electron injection rate from the unthermalized state to SnO_2 and ZnO than to TiO_2. The ET rate variation among these semiconductors is attributed to considerably lower density of states in the sp-type (SnO_2 and ZnO) than in d-type (TiO_2) conduction bands.

Acknowledgment. Financial support was provided by the Division of Chemical Sciences, Office of Basic Energy Research, U.S. Department of Energy. This work is also supported in part by the donors of the Petroleum Research Fund and the Emory University Research Committee. We are grateful to Dr. Robert P. Apkarian, the director of the Integrated Microscopy and Microanalytical Facility (IM&MF) and Dr. Encai Hao for SEM measurement. T.L. is an Alfred P. Sloan fellow.

References and Notes

(1) Miller, R. J. D.; McLendon, G. L.; Nozik, A. J.; Schmickler, W.; Willig, F. *Surface electron-transfer processes*; VCH Publishers, Inc.: New York, 1995.
(2) Kamat, P. V. *Chem. Rev.* **1993**, *93*, 267.
(3) Kamat, P. V. *Prog. React. Kinet.* **1994**, *19*, 277.
(4) Hagfeldt, A.; Gratzel, M. *Chem. Rev.* **1995**, *95*, 49.
(5) O'Regan, B.; Gratzel, M. *Nature* **1991**, *353*, 737.
(6) Bach, U.; Lupo, D.; Comte, P.; Moser, J. E.; Weissortel, F.; Salbeck, J.; Spreitzer, H.; Gratzel, M. *Nature* **1998**, *395*, 583.
(7) Nazeeruddin, M. K.; Kay, A.; Rodicio, I.; Humphrybaker, R.; Muller, E.; Liska, P.; Vlachopoulos, N.; Gratzel, M. *J. Am. Chem. Soc.* **1993**, *115*, 6382.
(8) Moser, J. E.; Bonnote, P.; Gratzel, M. *Coord. Chem. Rev.* **1998**, *171*, 245.
(9) Kay, A.; Gratzel, M. *Sol. Energy Mater. Sol. Cells* **1996**, *44*, 99.
(10) Asbury, J. B.; Anderson, N. A.; Hao, E.; Lian, T. *J. Phys. Chem. B* **2003**, *107*, 7376.
(11) Asbury, J. B.; Hao, E.; Wang, Y.; Ghosh, H. N.; Lian, T. *J. Phys. Chem. B* **2001**, *105*, 4545.
(12) Asbury, J. B.; Wang, Y. Q.; Hao, E. C.; Ghosh, H. N.; Lian, T. *Res. Chem. Interm.* **2001**, *27*, 393.
(13) Ellingson, R. J.; Asbury, J. B.; Ferrere, S.; Ghosh, H. N.; Sprague, J. R.; Lian, T.; Nozik, A. J. *Z. Phys. Chem. (Muenchen)* **1999**, *212*, 77.
(14) Asbury, J. B.; Ellingson, R. J.; Ghosh, H. N.; Ferrere, S.; Nozik, A. J.; Lian, T. *J. Phys. Chem. B* **1999**, *103*, 3110.
(15) Ellingson, R. J.; Asbury, J. B.; Ferrere, S.; Ghosh, H. N.; Sprague, J. R.; Lian, T.; Nozik, A. J. *J. Phys. Chem. B* **1998**, *102*, 6455.
(16) Tachibana, Y.; Haque, S. A.; Mercer, I. P.; Moser, J. E.; Klug, D. R.; Durrant, J. R. *J. Phys. Chem. B* **2001**, *105*, 7424.
(17) Tachibana, Y.; Moser, J. E.; Graetzel, M.; Klug, D. R.; Durrant, J. R. *J. Phys. Chem.* **1996**, *100*, 20056.
(18) Haque, S. A.; Tachibana, Y.; Willis, R. L.; Moser, J. E.; Graetzel, M.; Klug, D. R.; Durrant, J. R. *J. Phys. Chem. B* **2000**, *104*, 538.
(19) Hannappel, T.; Burfeindt, B.; Storck, W.; Willig, F. *J. Phys. Chem. B* **1997**, *101*, 6799.
(20) Benko, G.; Kallioinen, J.; Korppi-Tommola, J. E. I.; Yartsev, A. P.; Sundstrom, V. *J. Am. Chem. Soc.* **2002**, *124*, 489.
(21) Kalloinen, J.; Benko, G.; Sundstrom, V.; Korppi-Tommola, J. E. I.; Yartsev, A. P. *J. Phys. Chem. B* **2002**, *106*, 4396.
(22) Heimer, T. A.; Heilweil, E. J.; Bignozzi, C. A.; Meyer, G. J. *J. Phys. Chem. A* **2000**, *104*, 4256.
(23) Kuciauskas, D.; Monat, J. E.; Villahermosa, R.; Gray, H. B.; Lewis, N. S.; McCusker, J. K. *J. Phys. Chem. B* **2002**, *106*, 9347.
(24) Kuciauskas, D.; Freund, M. S.; Gray, H. B.; Winkler, J. R.; Lewis, N. S. *J. Phys. Chem. B* **2001**, *105*, 392.
(25) Fungo, F.; Otero, L.; Borsarelli, C. D.; Durantini, E. N.; Silber, J. J.; Sereno, L. *J. Phys. Chem. B* **2002**, *106*, 4070.
(26) Chappel, S.; Zaban, A. *Solar Energy Mater. Solar Cells* **2002**, *71*, 141.
(27) Sayama, K.; Sugihara, H.; Arakawa, H. *Chem. Mater.* **1998**, *10*, 3825.
(28) Stergiopoulos, T.; Arabatzis, I. M.; Cachet, H.; Falaras, P. *J. Photochem. Photobiol., A: Chem.* **2003**, *155*, 163.
(29) Bedja, I.; Kamat, P. V.; Hotchandani, S. *J. Appl. Phys.* **1996**, *80*, 4637.
(30) Bedja, I.; Hotchandani, S.; Kamat, P. V. *J. Phys. Chem.* **1994**, *98*, 4133.
(31) Ferrere, S.; Zaban, A.; Gregg, B. A. *J. Phys. Chem. B* **1997**, *101*, 4490.
(32) Miyasaka, T.; Watanabe, T.; Fujishima, A.; Honda, K. *J. Am. Chem. Soc.* **1978**, *100*, 6657.
(33) Bedja, I.; Hotchandani, S.; Carpentier, R.; Fessenden, R. W.; Kamat, P. V. *J. Appl. Phys.* **1994**, *75*, 5444.

(34) Otero, L.; Osora, H.; Li, W.; Fox, M. A. *J. Porphyrins and Phthalocyanines* **1998**, *2*, 123.
(35) Fungo, F.; Otero, L.; Durantini, E. N.; Silber, J. J.; Sereno, L. E. *J. Phys. Chem. B* **2000**, *104*, 7644.
(36) Hara, K.; Horiguchi, T.; Kinoshita, T.; Sayama, K.; Sugihara, H.; Arakawa, H. *Sol. Energy Mater. Sol. Cells* **2000**, *64*, 115.
(37) Barazzouk, S.; Lee, H.; Hotchandani, S.; Kamat, P. V. *J. Phys. Chem. B* **2000**, *104*, 3616.
(38) Tian, H.; Liu, P. H.; Meng, F. S.; Gao, E.; Cai, S. *Synth. Met.* **2001**, *121*, 1557.
(39) Sayama, K.; Hara, K.; Ohga, Y.; Shinpou, A.; Suga, S.; Arakawa, H. *New J. Chem.* **2001**, *25*, 200.
(40) Krishnan, M.; Zhang, X.; Bard, A. J. *J. Am. Chem. Soc.* **1984**, *106*, 7371.
(41) Fessenden, R. W.; Kamat, P. V. *J. Phys. Chem.* **1995**, *99*, 12902.
(42) Kamat, P. V.; Bedja, I.; Hotchandani, S.; Patterson, L. K. *J. Phys. Chem.* **1996**, *100*, 4900.
(43) Iwai, S.; Hara, K.; Murata, S.; Katoh, R.; Sugihara, H.; Arakawa, H. *J. Chem. Phys.* **2000**, *113*, 3366.
(44) Benko, G.; Myllyperkio, P.; Pan, J.; Yartsev, A. P.; Sundstrom, V. *J. Am. Chem. Soc* **2003**, *125*, 1118.
(45) Bauer, C.; Boschloo, G.; Mukhtar, E.; Hagfeldt, A. *Int. J. Photoenergy* **2002**, *4*, 17.
(46) Anderson, N. A.; Ai, X.; Chen, D.; Mohler, D. L.; Lian, T. *J. Phys. Chem. B* **2003**, *107*, 14231.
(47) Anderson, N. A.; Hao, E.; Ai, X.; Hastings, G.; Lian, T. *Chem. Phys. Lett.* **2001**, *347*, 304.
(48) Wang, Y.; Asbury, J. B.; Lian, T. *J. Phys. Chem. A* **2000**, *104*, 4291.
(49) Ghosh, H. N.; Asbury, J. B.; Weng, Y.; Lian, T. *J. Phys. Chem. B* **1998**, *102*, 10208.
(50) Nazeeruddin, M. K.; Zakeerudin, S. M.; Humphry-Baker, R.; Jirousek, M.; Liska, P.; Vlachopoulos, N.; Shklover, V.; Fischer, C.-H.; Gratzel, M. *Inorg. Chem.* **1999**, *38*, 6298.
(51) Ai, X.; Anderson, N. A.; Asbury, J. B.; Hao, E.; Lian, T. *Proc. SPIE Int. Soc. Opt. Eng.* **2003**, *5223*, 147.
(52) Ai, X.; Guo, J.; Anderson, N. A.; Lian, T. *J. Phys. Chem. B* **2004**, *108*, 12795.
(53) Redmond, G.; Fitzmaurice, D. *J. Phys. Chem.* **1993**, *97*, 1426.
(54) Shaw, G. B.; Papanikolas, J. M. *J. Phys. Chem. B* **2002**, *106*, 6156.
(55) Asbury, J. B.; Hao, E.; Wang, Y.; Lian, T. *J. Phys. Chem. B* **2000**, *104*, 11957.
(56) Anderson, N. A.; Ai, X.; Lian, T. *J. Phys, Chem. B* **2003**, *107*, 14414.
(57) Enright, B.; Fitzmaurice, D. *J. Phys. Chem.* **1996**, *100*, 1027.
(58) Enright, B.; Redmond, G.; Fitzmaurice, D. *J. Phys. Chem.* **1994**, *98*, 6195.
(59) Marcus, R. A. *J. Phys. Chem.* **1990**, *94*, 1050.
(60) Katoh, R.; Furube, A.; Yoshihara, T.; Hara, K.; Fujihashi, G.; Takano, S.; Murata, S.; Arakawa, H.; Tachiya, M. *J. Phys. Chem. B* **2004**, *108*, 4818.
(61) Marcus, R. A. *J. Chem. Phys.* **2000**, *113*, 1618.
(62) Gao, Y. Q.; Georgievskii, Y.; Marcus, R. A. *J. Chem. Phys.* **2000**, *112*, 3358.
(63) Gao, Y. Q.; Marcus, R. A. *J. Chem. Phys.* **2000**, *113*, 6351.
(64) Henrich, V.; Cox, P. *The Surface Science of Metal Oxides*; Cambridge University Press: Cambridge, U.K., 1996.
(65) Tachibana, Y.; Rubtsov, I. V.; Montanari, I.; Yoshihara, K.; Klug, D. R.; Durrant, J. R. *J. Photochem. Photobiol., A* **2001**, *142*, 215.
(66) Asbury, J. B.; Wang, Y.; Lian, T. *J. Phys. Chem. B* **1999**, *103*, 6643.
(67) Furube, A.; Katoh, R.; Hara, K.; Murata, S.; Arakawa, H.; Tachiya, M. *J. Phys. Chem. B* **2003**, *107*, 4162.
(68) Pankove, J. I. *Optical Processes in Semiconductors*; Dover: New York, 1975.
(69) Nelson, J.; Kirkpatrick, J.; Ravirajan, P. *Phys. Rev. B: Condens. Matter* **2004**, *69*, 035337.
(70) Boschloo, G.; Fitzmaurice, D. *J. Phys. Chem. B* **1999**, *103*, 3093.
(71) Bolts, J. M.; Wrighton, M. S. *J. Phys. Chem.* **1976**, *80*, 2641.
(72) Brown, G. M.; Sutin, N. *J. Am. Chem, Soc.* **1979**, *101*, 883.
(73) Marcus, R. A. Reorganization free energy for electron transfers at liquid−liquid and dielectric semiconductor-liquid interfaces. *J. Phys. Chem.* **1990**, *94*, 1050.
(74) Yonemoto, E. H.; Saupe, G. B.; Schmehl, R. H.; Hubig, S. M.; Riley, R. L.; Iverson, B. L.; Mallouk, T. E. *J. Am. Chem. Soc.* **1994**, *116*, 4786.
(75) Anderson, N. A.; Lian, T. *Coord. Chem. Rev.* **2004**, *248*, 1231.
(76) Sorantin, P. I.; Scharz, K. *Inorg. Chem.* **1992**, *31*, 567.
(77) Yu, P. Y.; Cardona, M. *Fundamentals of Semiconductors*, 2nd ed.; Springer-Verlag: Berlin, 1999.
(78) Redmond, G.; Fitzmaurice, D.; Graetzel, M. *J. Phys. Chem.* **1993**, *97*, 6951.